

Research Article

Properties of a Prototype Corium of Nuclear Reactor

Mazhyn K. Skakov,¹ Nurzhan Ye. Mukhamedov ,¹
Ilya I. Deryavko,¹ and Erlan G. Batyrbekov²

¹Institute of Atomic Energy, RSE NNC RK, Kurchatov, 071100, Kazakhstan

²National Nuclear Center RK, Kurchatov, 071100, Kazakhstan

Correspondence should be addressed to Nurzhan Ye. Mukhamedov; mukhamedov@nnc.kz

Received 19 April 2018; Revised 13 July 2018; Accepted 7 August 2018; Published 2 September 2018

Academic Editor: Alejandro Clause

Copyright © 2018 Mazhyn K. Skakov et al. This is an open access article distributed under the Creative Commons Attribution License, which permits unrestricted use, distribution, and reproduction in any medium, provided the original work is properly cited.

The paper studies structure, phase composition, and thermophysical properties (TPP) (specific heat capacity, thermal diffusivity, and heat conductivity) of a prototype corium of a fast nuclear reactor (melt of core materials of nuclear reactor produced under out-of-pile conditions). The obtained data will be used to get more accurate understanding of main regularities of actual interaction of core materials of a nuclear reactor under a severe accident.

1. Introduction

In order to solve issues for studying processes occurring under in severe accidents in nuclear reactor and to research properties of generated alloys and compounds, the most efficient instrument is physical simulation, which simulates real processes at the laboratory conditions and enables to obtain data that can be applied for solving of actual problems.

As a rule, model physical objects are usually being produced in accordance with a certain similarity to full-scale ones.

At the practice, methods of physical simulation are used for

- (i) studying gas fluxes and airflow of flying machines, vehicles, and others in wind tunnels;
- (ii) hydrodynamical studying of hydraulic structures, ships, and others;
- (iii) determining seismic resistance of structures at their mock-ups;
- (iv) studying resistance of complex structures under effect of complex power loads;
- (v) measuring thermal fluxes and heat dissipations in devices and systems operating under conditions of complex power loads;

- (vi) studying of natural phenomena and their consequences.

Experimental works on physical modeling of severe accidents are conducted in many research centers over the world [1]. For example, the studies of accidents within the following programs are PHEBUS [2], CORA [3], CODEX [4], KROTOS [5], «RASPLAV» [6], MACE [7], FARO/TERMOS [8], FRAG [9], Betulla [10], CORRECT [11], and VITI [12]. Most of the experiments are aimed at obtaining knowledge on the processes occurring at various stages of severe accidents [13, 14].

Within the above studies, the Institute of Atomic Energy Branch of the National Nuclear Center of the Republic of Kazakhstan conducts both in-pile [15–17] and out-of-pile [18, 19] experiments to study behavior of energy nuclear reactor fuel under the conditions of severe accident with loss of coolant (LOCA).

The purpose of this work is experimental research of properties and structure of molten core materials of a nuclear reactor produced by induction heating at VCG-135 test bench.

2. The Research Materials and Methods

A corium ingot resulted from out-of-pile experiment through induction heating of materials in a graphite crucible with



FIGURE 1: VCG-135 test bench.

tantalum carbide protecting insert at VCG-135 test bench and was selected as research material.

The VCG-135 test bench is designed for high-temperature material studies into the processes of interaction of reactor core components when they are heated as high as melting temperature.

The VCG-135 test bench is created based on a VCG-60/0.066 high frequency electric generator and a hermetically sealed, water-cooled process chamber with an inbuilt inductor, and it is designed for high-temperature and thermophysical and materials testing on small materials samples. The bench is illustrated in Figure 1. The bench facilitates the controlled heating of any small samples to high temperature (3,000°C) with subsequent cooling using heat lakes to the water-cooled inductor when the generator is powered down [20].

The bench facilitates a wide range of experimental studies with the heating of reactor core materials, right up to their pouring point, including the following:

- (i) study of the interaction of corium components during their heating, right up to pouring point;
- (ii) study of effectiveness of different kinds of graphite crucible protection based on carbides of Zr, Nb, Ta, and others;
- (iii) determination of phase transfer temperatures in corium of various compositions;
- (iv) study of the high-temperature interaction of corium with structural materials (ceramics, alloys);
- (v) determinations of the electrophysical properties of corium;
- (vi) obtaining compact corium ingots of the set composition.

Technical specifications of VCG-135 are

- (i) generator frequency, 66 kHz;
- (ii) internal diameter of process chamber, 600 mm;
- (iii) height of process chamber, 700 mm;
- (iv) inductor dimensions, $\text{Ø}80 \times 150$ mm, $\text{Ø}120 \times 150$ mm;
- (v) temperature sensors: thermocouples, pyrometers;
- (vi) gaseous medium in the process chamber: vacuum, argon;
- (vii) mass of loaded charge material, 100-500 g.

TABLE 1: The chemical composition of the used steels (wt. %).

(a)									
12Cr18Ni10Ti stainless steel									
Fe	C	Cr	Ni	Ti	Si	Mn	P	S	
base	0.12	18.24	10.07	0.39	0.34	1.67	0.032	0.013	
(b)									
Cr16Ni15Mo3Nb steel									
Fe	C	Cr	Ni	Nb	Si	Mn	P	S	Mo
base	0.09	16	15	0.9	0.8	0.8	0.035	0.02	3

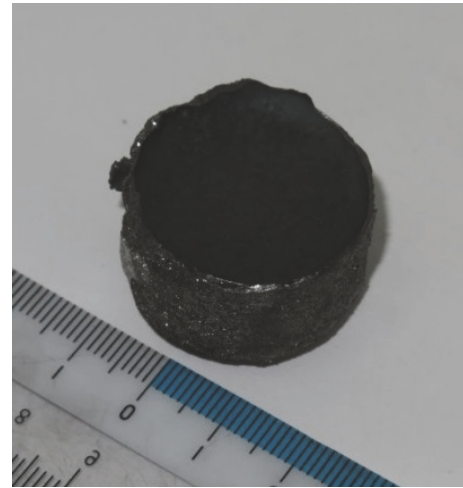


FIGURE 2: Physical configuration of corium ingot.

The bench makes provision for video recording of the heating and cooling of the studied sample through a viewing window in the top of the process chamber and also the ability to sample the gas during the experiment. The bench's process chamber is equipped with standby electrical cable passes for various electrical measurements during the course of the experiment. Standby gas flanges and connecting branches are available to expand capabilities and to adapt to new tasks that may be addressed on the bench.

To obtain the corium prototype, a method described in [18] was used. The burden loaded into this crucible contained 135.01 g of uranium dioxide pellets with 0.27% U^{235} enrichment, 8.51 g of Cr16Ni15Mo3Nb stainless steel (foreign analogues of Cr16Ni15Mo3Nb steel are 318 (USA) and X10CrNiMoNb18-12 (Germany)), and 1.51 g of 12Cr18Ni10Ti stainless steel (foreign analogues of 12Cr18Ni10Ti steel are 321 (USA) and X10CrNiTi18-10 (Germany)). The chemical composition of the used steels is shown in Table 1. A compact ingot of the prototype corium resulted from the experiment; its physical configuration is shown in Figure 2. A disk-shaped sample (Figure 3) was cut out for further research.

Measurement of thermophysical properties of produced corium was carried out on thin disk samples prepared for the conditions of the laboratory installation of thermophysical measurements of UTFI-2 in the IAE Branch NNC RK.

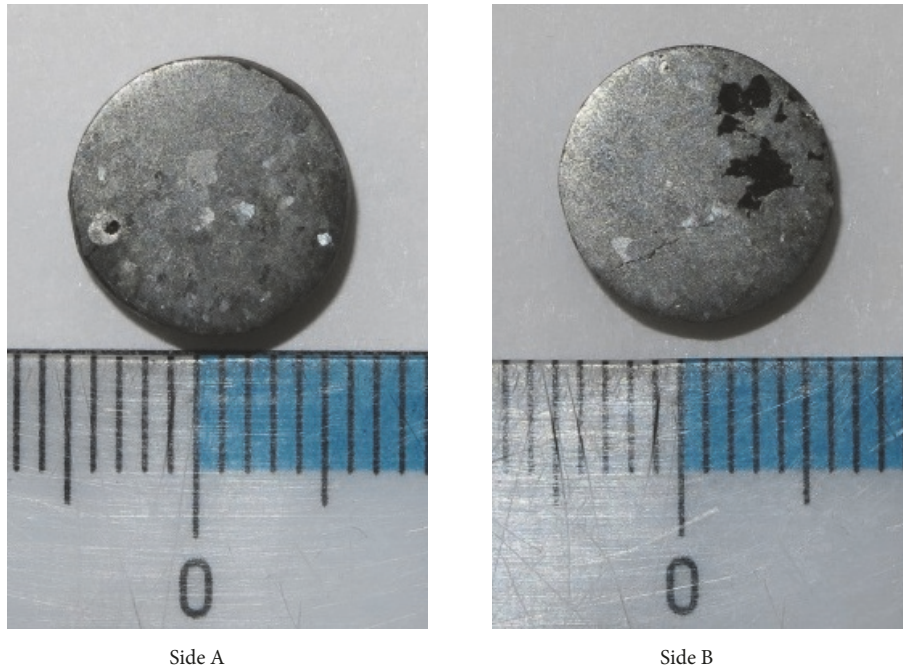


FIGURE 3: Physical configuration of sample.



FIGURE 4: Laboratory installation of thermophysical measurements of UTFI-2.

Structurally, the installation consists of an instrument rack of the information and measuring system (IMS), a measuring cell (conductivity meter), and a vacuum chamber with a heating unit and a recording system for operating the heating unit. Vacuum chamber with vacuum and inert gas filling system, power section, and measuring circuit of the heating unit are assembled into one functional unit based on vacuum universal post VUP-1. General view of the installation is shown in Figure 4.

X-ray structural corium researches were conducted on Empyrean diffractometer with Roentgen-Master controlling computer system. X-rayograms were obtained by means of monochromated $\text{CuK } \alpha$ -radiation ($\lambda_{\text{K}\alpha 1} = 0.154056 \text{ nm}$) under accelerating voltage of 30 kV and anode current of 40 mA with scanning interval with angle of 2θ : 30° - 120° and stride of 0.02° .

X-rayogram transcript was carried out by Crystallography Open Database (COD) [21].

The structure and element composition of the corium were studied in a JSM-6390 scanning electron microscope equipped by a JED-2300 energy-dispersive spectrometer (EDS).

3. The Research Results and Their Discussion

Figure 5 shows typical macro- and microstructures of the corium. The surface of material is characterized by small cracks. As the experiment result, molten metal veins separate the main matrix of the material during the solidification.

The structure analysis allowed establishing the following. The matrix structure of such material is single-phase, porous, and with cracks. Therewith, the metal phase in micropores of several micrometers is quite evenly distributed in the material matrix, as it can be seen in the optical metallography images. It can be assumed that these almost spherical particles of the metallic phase appeared as a result of local boiling processes of steel particles in a liquid matrix from the material heated to high temperatures exceeding the steel boiling temperature.

Figure 6 shows typical surface microstructure. SEM images were obtained with x500 zooming.

The corium surface microstructure is characterized by the presence of metallic inclusions and veins separating the grains of the main matrix. The size of the inclusions is $10 \div 15 \mu\text{m}$, which indicates the nondissolution of steel in the ceramic matrix of uranium dioxide. For the identification of the elemental composition of the samples of the solidified melt, an EDS analysis of the entire surface of the obtained corium sample was carried out. The data of the elemental composition in mass percent are presented in Table 2. According to the obtained data of elemental analysis, it is determined that the material mainly consists of uranium. The presence of tantalum in the results of elemental analysis is explained by the technology of manufacturing a corium ingot. Presumably, when removing the corium ingot, the particles of the protective glass are embedded on the ingot; thereby tantalum is displayed on the results of the EDS analysis.

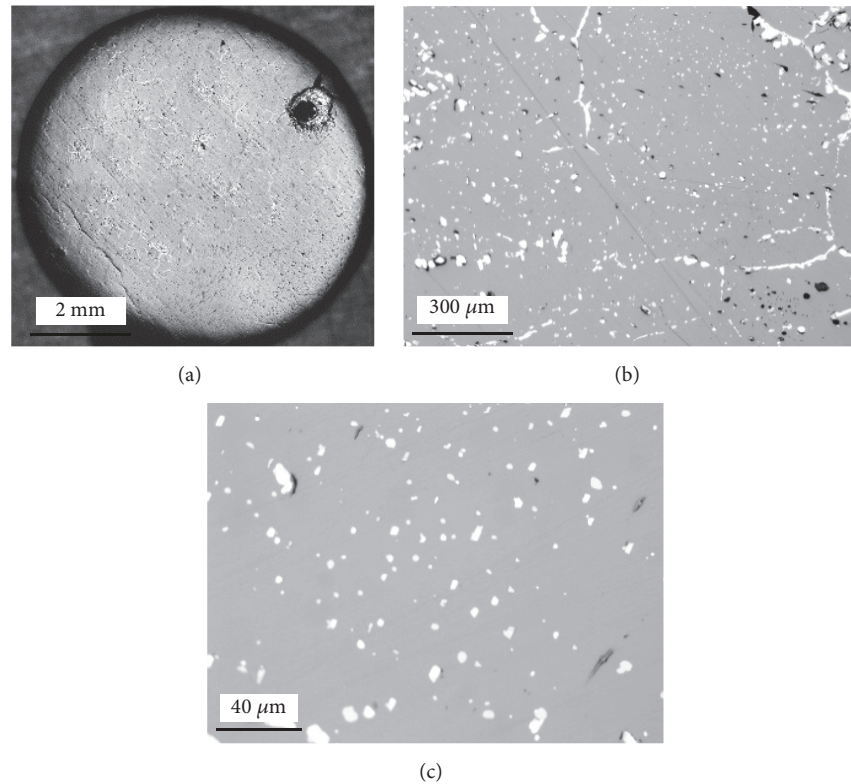


FIGURE 5: Macro- (a) and microstructure (b, c) of the corium.

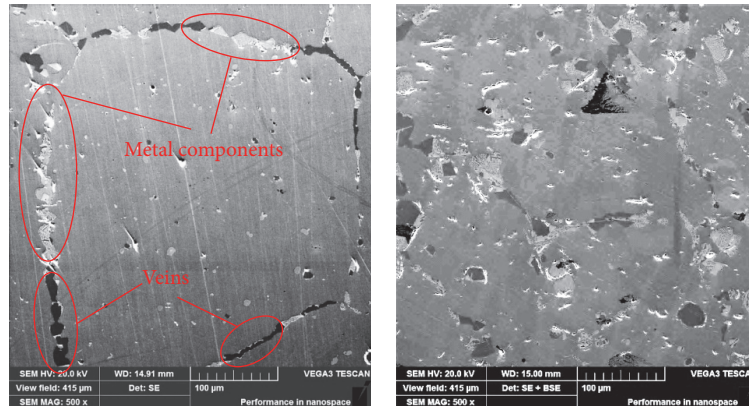


FIGURE 6: Microstructure of the corium material surface.

Based on the results of elemental analysis, the average value of the metallic inclusion on the surface of the corium sample is approximately 1.75% (by weight), with the initial charge of steel in the burden being 6.9%. Presumably, during the melting experiment of the charged burden, the first melting of the steel and then the melting of the fuel pellets occurred. After the complete melting of the uranium dioxide pellets, the fuel melt moved to the bottom of the graphite melting crucible, squeezing the melt of the steel upwards. During extrusion, the melts were stirred, and the effervescence of the steel particles inside the ceramic matrix occurred. When the mixture of the melt of fuel and steel cools, the fuel melt solidifies first, without letting the entire steel

bulge upwards. Such a hypothetical, in our opinion, sequence of melting and solidification processes allows explaining the decrease in the percentage ratio of steel on the surface of the corium sample.

The diffraction pattern analysis (Figure 7) revealed UO_2 with face-centered cubic lattice as the main crystalline phase. On the diffraction patterns, the main phase peaks are narrow with well-resolved $K\alpha_{1,2}$ -doublet at 2θ more than 50° angles indicating a sufficiently high perfection of the structure of the main phase crystal lattice. The calculations of the crystal lattice period were performed using the diffraction patterns processing results. The average value of the lattice period was $a_0 = (0.5472 \pm 0.0002)$ nm.

TABLE 2: Elemental analysis results.

Element	O	Ti	Cr	Fe	Ni	Ta	U
Maximum value, %	15.38	0.29	0.3	1.08	0.3	0.72	82.94
Minimum value, %	15.03	0.25	0.21	0.81	0.15	0.48	82.23
Average value, %	15.19	0.27	0.25	0.98	0.25	0.59	82.48

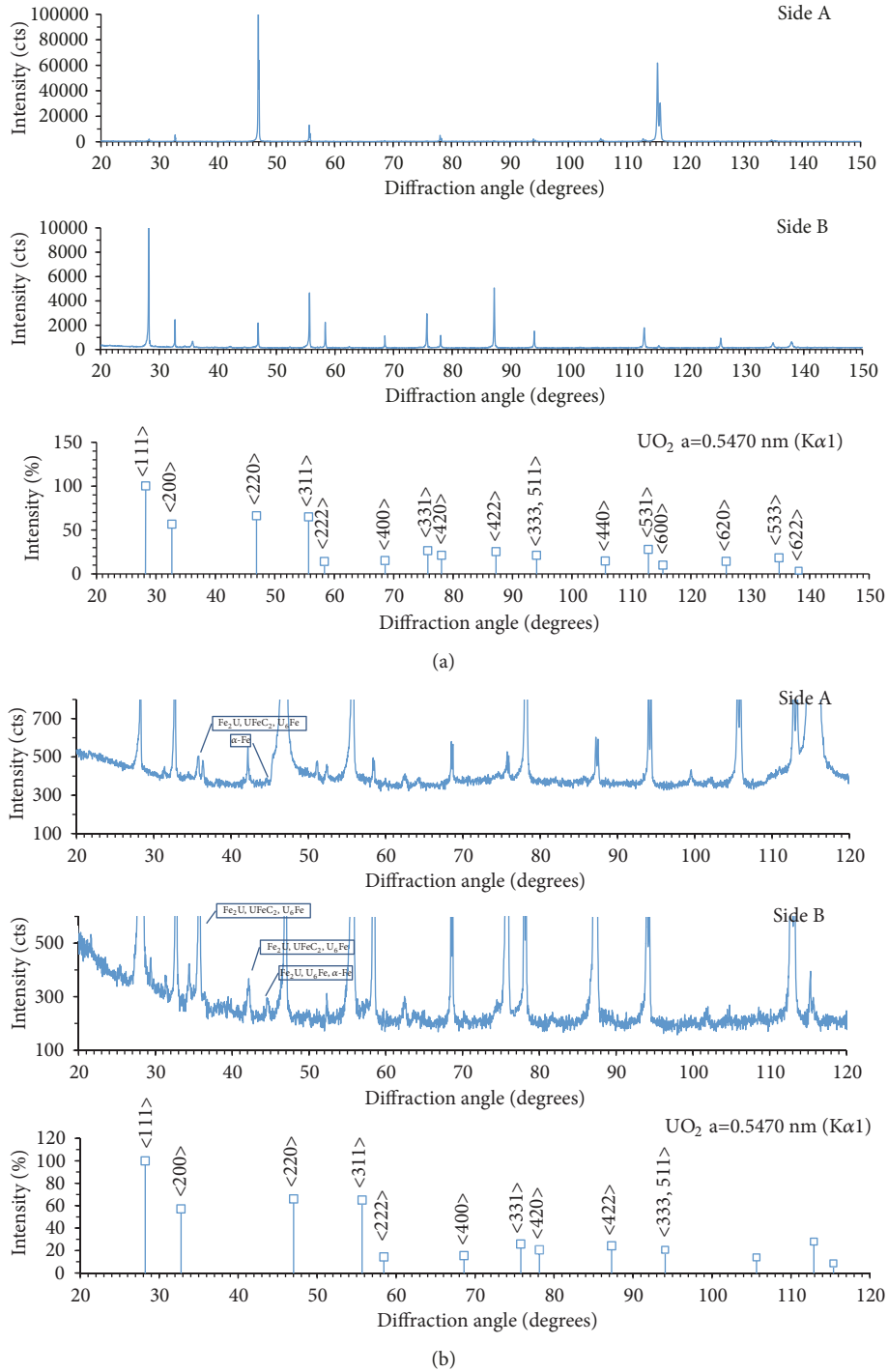


FIGURE 7: Diffraction pattern with identified peaks (a, in full scale; b, for low intensity lines).

TABLE 3: The results of temperature measuring of TPP coefficients.

	Temperature, °C	Pulse energy, J	TPP coefficients		
			$a, 10^{-6} \text{ m}^2/\text{sec}$	$C, \text{ J}/(\text{kg}\cdot^\circ\text{C})$	$\lambda, \text{ W}/(\text{m}\cdot^\circ\text{C})$
1 st cycle, heating					
1	21.4±0.5	13.92±0.05	3.168±0.010	233.1±0.8	8.24±0.05
2	98.7±0.5	13.14±0.02	2.940±0.004	247±2	8.10±0.08
3	202.0±0.9	16.9±0.3	2.554±0.007	289±3	8.22±0.07
4	300.6±0.2	16.55±0.2	2.306±0.011	305.1±1.5	7.85±0.05
5	302.5±0.4	16.59±0.05	2.300±0.016	305.6±0.3	7.84±0.06
6	299.8±0.4	16.41±0.09	2.289±0.005	305.8±1.7	7.81±0.03
7	345.21±0.06	16.15±0.07	2.188±0.017	315±3	7.676±0.018
8	404.1±	16.0±0.17	2.104±0.012	323.4±0.8	7.59±0.06
1 st cycle, cooling					
9	348.4±1.2	16.48±0.07	2.19±0.03	317.5±0.6	7.76±0.07
10	28.9±0.4	13.68±0.11	3.085±0.013	245.0±1.0	8.43±0.06
2 nd cycle, heating					
1	23.6±0.4	13.28±0.15	3.094±0.003	242.4±0.9	8.37±0.02
2	105.6±0.4	12.83±0.05	2.801±0.014	271.2±1.9	8.47±0.10
3	197.7±0.5	14.33±0.08	2.508±0.010	295.8±0.6	8.27±0.03
4	299.0±0.9	16.36±0.10	2.277±0.004	310±3	7.87±0.05
5	303.6±1.2	16.54±0.10	2.246±0.005	308±3	7.74±0.07
6	352.3±0.4	16.18±0.10	2.16±0.02	321.9±1.0	7.75±0.09
7	400.1±0.5	15.85±0.11	2.061±0.008	330±3	7.59±0.07
8	453.5±0.1	19.3±0.2	1.99±0.03	343.3±1.1	7.62±0.08
9	511.3±0.7	19.27±0.14	1.897±0.016	358±4	7.58±0.03
2 nd cycle, cooling					
10	453.1±1.4	19.27±0.14	1.934±0.008	361±2	7.79±0.08
11	385.0±1.0	15.99±0.13	2.001±0.008	362±3	8.08±0.09
12	300.5±0.2	16.62±0.10	2.125±0.004	353±4	8.38±0.09
13	22.2±0.6	13.04±0.09	2.814±0.005	279.3±1.7	8.76±0.06

It was found that the material is characterized by a highly heterogeneous structure with large grains (the distributions of the lines intensity within each diffraction pattern had significant deviations from the equilibrium; different lines correspond to the maximum intensities, both within each end and between the ends in general).

The presence of weak lines of the second $U_6\text{Fe}$ phase with a tetragonal lattice, in which content in the samples reaches 4% (by mass), was also found on the diffraction patterns in addition to the main phase lines.

Table 3 shows the results of TPP measuring of the corium performed at the temperature range from 21°C up to 500°C.

The results of TPP measuring in the heating cycle showed insignificant changes while measuring at the cooling phase in the first heating cycle up to 400°C. First, the values of heat conductivity have been changed. The TPP values, which were measured at the both start and end of the heating cycle at room temperature, differ by 4% maximum.

During the heating stage of the second cycle TPP values in the temperature range up to 400°C and values resulted from the first cycle were the same. In the temperature dependencies, there is a changing of tendency after achieving

the temperature point of 400°C. The measure results showed significant changes in measurements during the cooling stage in the second heating cycle up to 511°C. The values of both heat conductivity and heat capacity were changed. The TPP values, which were measured at the start and at the end of heating cycle at room temperature, differ by 10% for thermal diffusivity, 13% for heat capacity, and 4.5% for heat conductivity. Heat conductivity and thermal diffusivity have reproducible tendencies of the temperature decreasing to 400°C.

4. Conclusion

It has been established that the corium is formed by mutual mixing of liquid uranium dioxide and liquid steels. The following conclusions were drawn while characterizing macro- and microstructures and determining the corium element composition:

- (i) The sample macrostructure is characterized by almost complete absence of macrocracks and the presence of macropores (porosity level ~20%).

- (ii) The sample microstructure contains metallic inclusions with dimensions from 10 to 15 μm .
- (iii) According to element analysis, the sample materials consist mainly of uranium dioxide, and at the same time the content of elements in steel is small.
- (iv) Based on X-ray phase analysis it was established that UO_2 is the main structural component and the second structural component is U_6Fe phase.

Data Availability

The data used to support the findings of this study are available from the corresponding author upon request.

Conflicts of Interest

The authors declare that there are no conflicts of interest regarding the publication of this paper.

Acknowledgments

The research was supported by the Committee of Science of the Ministry of Education and Science of the Republic of Kazakhstan for 2018 “Properties and Characteristics of the Core Material Melt of Nuclear Reactor Produced in IGR Research Reactor” (Contract No. 305 dated 30.03.2018).

Supplementary Materials

The X-ray diffraction data are attached in the attachment. (*Supplementary Materials*)

References

- [1] D. Jacquemain, “Nuclear Power Reactor Core Melt Accidents,” *IRSN*, 2015.
- [2] A. B. Anderson, A. Auvinen, P. D. W. Bottomley et al., “Revapourisation tests on samples from Phebus FP: final report,” in *European Commission 4th framework programme, Report ST: RVP(00)-P029*, Report ST, RVP(00)-P029, 2000.
- [3] S. Hagen, P. Hofmann, V. Noack, L. Sepold, G. Schanz, and G. Schumacher, “Comparison of the quench experiments CORA12, CORA13,” *Tech. Rep.*, 1996.
- [4] L. Jaffe, W. M. Bland Jr., R. English et al., “Reports of the technical assessment task force on chemistry, thermal hydraulics, core damage; WASH 1400,” *Reactor safety study; Alternative event sequences*, vol. 2, p. 236, 1979.
- [5] I. Huhtiniemi and D. Magallon, “Insight into steam explosions with corium melts in KROTOS,” *Nuclear Engineering and Design*, vol. 204, no. 1–3, pp. 391–400, 2001.
- [6] F. Fichot, V. Kobzar, V. Zvonarev, and P. Bousquet Mélou, “The Use of RASPLAV Results in IPSN Severe Accident Research Program, in OECDNEA Proceedings of RASPLAV Seminar,” in *Proceedings of the The Use of RASPLAV Results in IPSN Severe Accident Research Program, in OECDNEA Proceedings of RASPLAV Seminar*, Munich, 2000.
- [7] M. T. Farmer, B. W. Spencer, J. L. Binder, and D. J. Hill, “Status and Future Direction of the Melt Attack and Coolability Experiments (MACE) Program at the Argonne National Laboratory,” in *Proceedings of 9th International Conference on Nuclear Engineering, ICONE-9697*, April 2001.
- [8] D. Magallon, H. Hohmann, and H. Schins, “Pouring of 100-kg-scale molten UO_2 into sodium,” *Nuclear Technology*, vol. 98, no. 1, pp. 79–90, 1992.
- [9] T. Y. Chu, “Fragmentation of molten-core material by sodium , International topical meeting on LMFBR safety,” in *Proceedings of the International topical meeting on LMFBR safety, SAND-82-0300C; CONF-820704-10*, p. 82, Lyon, France, 1982.
- [10] H. Schins and F. S. Gunnerson, “Boiling and fragmentation behaviour during fuel-sodium interactions,” *Nuclear Engineering and Design*, vol. 91, no. 3, pp. 221–235, 1986.
- [11] G. Berthoud, “Vapor explosions,” *Annual Review of Fluid Mechanics*, vol. 32, pp. 573–611, 2000.
- [12] K. Plevacova, C. Journeau, P. Piluso, and J. Poirier, “Eutectic crystallization in the $\text{UO}_2\text{-Al}_2\text{O}_3\text{-HfO}_2$ ceramic phase diagram,” *Ceramics International*, vol. 40, no. 2, pp. 2565–2573, 2014.
- [13] B. R. Sehgal, T. N. Dinh, V. A. Bui, J. A. Green, and G. Kolb, “SIMECO Experiments on in-vessel melt pool formation and heat transfer with and without a metallic layer,” in *Proceeding of OECD Workshop on ex-vessel*, pp. 198–206, Germany: Garching, 1998.
- [14] O. N. Kashinsky, P. D. Lobanov, N. A. Pribaturin, A. S. Kurdyumov, and S. E. Volkov, “Experimental study of the effect of the spacing lattice on the flow structure in the fuel assemblies of the NPP-2006 reactor,” *Teploenergetika*, vol. 1, pp. 63–67, 2013.
- [15] M. K. Skakov, N. Y. Mukhamedov, A. D. Vurim, and I. I. Deryavko, “Temperature Dependence of Thermophysical Properties of Full-Scale Corium of Fast Energy Reactor,” *Science and Technology of Nuclear Installations*, vol. 2017, 2017.
- [16] M. Skakov, N. Mukhamedov, I. Deryavko, W. Wieleba, and A. Vurim, “Research of structural-phase state of natural corium in fast power reactors,” *Vacuum*, vol. 141, pp. 216–221, 2017.
- [17] M. K. Skakov, N. Y. Mukhamedov, I. I. Deryavko, and I. M. Kukushkin, “Thermal properties and phase composition of full-scale corium of fast energy reactor,” *Key Engineering Materials*, vol. 736, pp. 58–62, 2017.
- [18] N. Mukhamedov, M. Skakov, I. Deryavko, and I. Kukushkin, “Thermal properties of prototype corium of fast reactor,” *Nuclear Engineering and Design*, vol. 322, pp. 27–31, 2017.
- [19] M. Skakov, N. Mukhamedov, W. K. Wieleba, and I. Deryavko, “Study of corium thermophysical properties of light water reactor with different oxidation degrees of zirconium,” *Research Journal of Pharmaceutical, Biological and Chemical Sciences*, vol. 7, no. 4, pp. 2018–2024, 2016.
- [20] V. Zhdanov, “Facility for LWR Core Materials Studies at High Temperature,” in *Proceedings of ICAPP05 congress / V.V. Zhdanov*, pp. 15–19, Seoul, Korea, 2005.
- [21] S. Graulis, D. Chateigner, R. T. Downs et al., “Crystallography Open Database - an open-access collection of crystal structures,” *Journal of Applied Crystallography*, vol. 42, pp. 726–729, 2009.

